Transformation between Inverse Bicontinuous Cubic Phases of a Lipid from Diamond to Gyroid

Langmuir

Article

pubs.acs.org/Langmuir

Transformation between Inverse Bicontinuous Cubic Phases of a Lipid from Diamond to Gyroid

Toshihiko Oka*

Department of Physics, Faculty of Science and Nanomaterials Research Division, Research Institute of Electronics, Shizuoka University, Shizuoka 422-8529, Japan

Supporting Information

ABSTRACT: The transformation between inverse bicontinuous cubic phases of a lipid from diamond (Q_{II}^{D}) to gyroid (Q_{II}^{G}) in the single crystal region of monoolein was studied. X-ray diffraction data indicate that the single orientation of the Q_{II}^{D} phase was converted into an almost single orientation of the Q_{II}^{G} phase. The [111] and [1$\bar{1}$0] directions of a single crystal of the Q_{II}^{D} phase corresponded to the [202] and [0$\bar{4}$0] directions of the Q_{II}^{G} phase, respectively. This orientation relationship indicated that one direction in the four-branched water channels of the Q_{II}^{D} phase was preserved in the three-branched water channels of the Q_{II}^{G} phase. Using this relationship, a transformation model was constructed in which one direction of the water channels was preserved while another direction appeared.

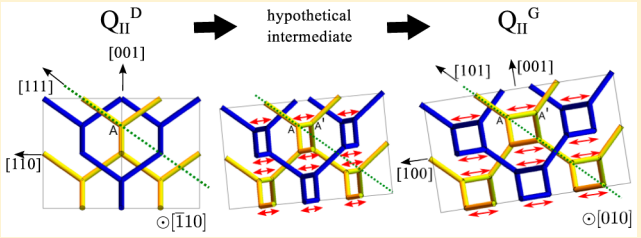

INTRODUCTION

A triply periodic minimal surface (TPMS) has an infinitely extending structure and separates space into two interwoven network structures[1,2] (Figure 1). Three types of TPMSs, viz., gyroid (G), diamond (D), and primitive (P) TPMSs, which have cubic symmetry and belong to the crystallographic space groups $Ia\bar{3}d$, $Pn\bar{3}m$, and $Im\bar{3}m$, respectively, are frequently observed in natural and artificial material systems, like lyotropic liquid crystals,[3,4] diblock copolymers,[5] prolamellar bodies of plants,[6] the organized smooth endoplasmic reticulum,[7] and butterfly wing scales.[8] Inverse bicontinuous cubic (Q_{II}) phases formed in lipid−water systems are examples of TPMSs found in natural and artificial material systems in which Q_{II} phases having gyroid (Q_{II}^{G}), diamond (Q_{II}^{D}), and primitive (Q_{II}^{P}) structures have been observed.[3]

Phase transitions between Q_{II} phases are frequently observed in lipid−water systems[3,4] and recently in diblock copolymers.[9−11] However, the transformation mechanism of the lipid membrane during the phase transition is unclear. Simple theoretical mechanisms for the transformations between the three TPMSs were reported as involving the merging and separation of junctions of interwoven network labyrinths.[12,13] It has also been shown that the transformations between all three TPMS structures can preserve both topology and zero mean curvature throughout.[14] Two pathways, namely, tetragonal and rhombohedral pathways, were proposed for the transformation between G and D.[14,15] In experimental studies on the transformations in natural or artificial material systems, it is important to know the orientation (or epitaxial) relationships between before and after the phase transitions to deduce the transformation pathway. Several techniques have been reported in lipid/water systems to control the crystallographic orientation of the Q_{II} phases on a flat surface or a capillary wall[16,17] and applied to research on the phase transition from Q_{II}^{G} to Q_{II}^{D}.[17,18] Seddon et al. showed that the tetragonal pathway was adequate to explain their X-ray diffraction data on the Q_{II}^{D}−Q_{II}^{G} transition. But only one direction of the crystal orientation can be aligned by these techniques, and thus it seems difficult to show clear orientation relationships in the transformations between the Q_{II} phases. Therefore, my group developed a method to make a single crystallized region of the Q_{II}^{D} phase[19] that clearly showed the crystallographic orientation of the Q_{II}^{D} phase. Using this method, I already determined the orientation relationship in the Q_{II}^{D}-to-Q_{II}^{P} phase transformation and constructed a transformation model that preserved one direction of water channels.[20] In the present paper, I studied the phase transition from Q_{II}^{D} to Q_{II}^{G} in the single crystal region and found the same rule as in the Q_{II}^{D}−Q_{II}^{P} transition, i.e., that one direction of water channels was preserved during the phase transition.

MATERIALS AND METHODS

The single crystal region of the Q_{II}^{D} phase was prepared according to a procedure reported previously.[19,20] A 80:20 v/v solution of water/*tert*-butyl alcohol (Wako Pure Chemical Industries, Osaka, Japan) was prepared. The solution was mixed with dried monoolein (1-oleoyl-*rac*-glycerol) (Sigma Chemical Co., St. Louis, MO) in a 60:40 w/w solvent/monoolein ratio. The sample was loaded into a polyimide capillary (PIT-S, Furukawa Electric Co., Tokyo, Japan). One end of the sample was sealed with a tube sealing compound (Chaseal, Chase Scientific Glass, Rockwood, TN), while the other end was soaked in

Received: June 14, 2015
Revised: September 24, 2015
Published: October 1, 2015

DOI: 10.1021/acs.langmuir.5b02180
Langmuir 2015, 31, 11353−11359

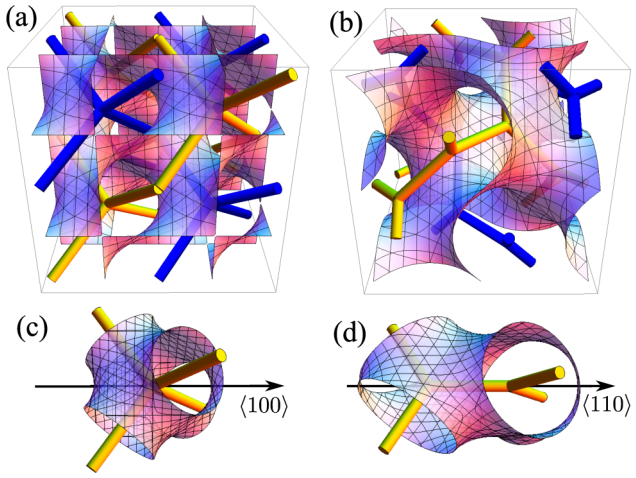

Figure 1. (a) TPMS structures of D. Unit cells of 2 × 2 × 2 are drawn. (b) TPMS structures of G. A single unit cell is drawn. The TPMS separates space into two interwoven regions. Two different tones of pipes indicate the centers of the two interwoven regions. In the structure of the Q_{II} phases of a lipid, the TPMS positions are occupied by a lipid bilayer membrane, and the two interwoven regions are occupied by water. (c) One four-way junction of interwoven region in D. (d) Two adjacent three-way junctions of interwoven regions in G. The one four-way junction of D separates into two three-way junctions of G in the D−G transformation model with tetrahedral symmetry. In this model, the transformation is obtained by pulling along one of the ⟨100⟩ directions of D, and a new pipe appears in G. The direction in which the new pipe appears corresponds to one of the ⟨100⟩ directions of G.

water at 25 °C. After about 2 months, the powder region of the sample was cut off, and the remaining part was transferred into a 20% poly(ethylene glycol) 4000 (PEG-4K) (Sigma-Aldrich Co., St. Louis, MO) solution. After 1 day, X-ray diffraction was performed.

X-ray diffraction measurements were conducted in almost the same manner as in my previous paper,[19,20] i.e., using a small-angle X-ray scattering system (NANO-Viewer system, Rigaku, Tokyo, Japan). The diameters of the three pinholes of the system were 0.6, 0.4, and 0.7 mm. The system was run at 40 kV and 30 mA. X-ray diffraction patterns were measured using a two-dimensional detector (PILATUS 100 K, Dectris, Baden, Switzerland). The detector was placed on a *z*-axis stage. Two images at different *z*-positions were merged into one large image. The sample−detector distance was set to 493 mm. Measurements were performed at 25 °C. To measure X-ray diffractions, I used the rotating crystal method. The sample, which was rotated from 0 to 180° in increments of 2°, was exposed to X-rays for 20 s at each step. To study the orientation relationship between the two phases, X-ray diffraction data were measured around the phase transition interface by changing the sample height. The method used to analyze the diffraction data was almost the same as that reported previously.[20] Using the diffraction peak positions, rotational matrices of the crystal orientations of Q_{II}^{D} (R_D) and Q_{II}^{G} (R_G) were calculated from the base coordinate. In the data for the Q_{II}^{D} phase, diffraction spots from the {110}, {111}, {200}, {211}, {220}, {221}, and {222} planes were used in the calculations. In the case of the Q_{II}^{G} phase, spots from the {211}, {220}, and {400} planes were used. The rotational matrices R_D and R_G were used to calculate the peak positions of unobservable diffraction spots in the extinction rules, and then the phase of the sample was identified. The rotational matrix from Q_{II}^{D} to Q_{II}^{G}, R_{DG}, was calculated via $R_{DG} = R_D^{-1}R_G$. A rotational matrix is defined by a rotational axis and a rotational angle.[21] The rotational axis of R_{DG} is an eigenvector of the matrix. The rotational angle, θ, around the rotational axis was calculated from the trace of R_{DG} via $1 + 2\cos\theta = \mathrm{Tr}\, R_{DG}$. The crystal systems of the Q_{II}^{D} and Q_{II}^{G} phases are cubic, in which the three axes are equivalent. Thus, there are uncertainties in assigning the Miller indices. I selected the axes sets and Miller indices in the two phases that would facilitate comparison of my model with previously reported models.

I constructed a model of a hypothetical intermediate in Figure 5c in the same manner as in my previous paper.[20] I aligned the orientations of 1 four-way junction of the Q_{II}^{D} phase and 2 three-way junctions of the Q_{II}^{G} phase. Next, I calculated and defined the midpoint of the respective junctions of the Q_{II}^{D} and Q_{II}^{G} phases as the hypothetical intermediate. Then, I calculated the periodical structure of the intermediate using the periodicity of the Q_{II}^{D} and Q_{II}^{G} phases.

RESULTS

Figure 2 illustrates the sample preparation method. To obtain a long single crystal region of monoolein in a capillary, I used a method reported previously by my group.[19,20] X-ray diffraction of the sample indicated that the length of the single crystal region was about 15 mm (data not shown). High-molecular-weight PEG solutions are known to convert the Q_{II}^{D} phase of monoolein into the Q_{II}^{G} phase.[22−24] The open end of the capillary sample was soaked in 20% PEG-4K to change the phase of the single crystal. Thus, the PEG-4K solution led to a gradual Q_{II}^{D}−Q_{II}^{G} phase transition from the open end. After 1 day of soaking in PEG-4K solution, I obtained X-ray diffraction patterns of the sample at different distances from the open edge. The single crystal region near the open edge was transformed into the Q_{II}^{G} phase, but far from the edge, the Q_{II}^{D} phase remained.

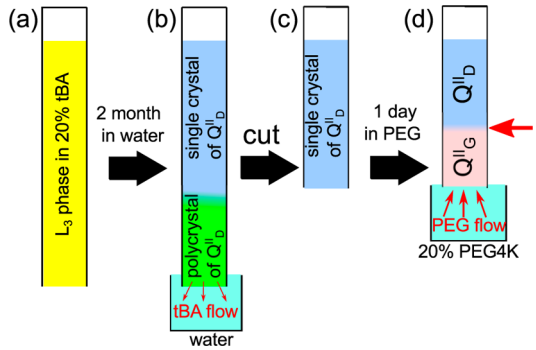

Figure 2. Schematic of the sample preparation process. (a) Monoolein sample before soaking in water. Concentration of *tert*-butyl alcohol (tBA) was 20%. The phase of monoolein was L_3. (b) Sample was soaked in water for 2 months. The tBA in the capillary diffused out gradually from the open edge, and a single crystal region of Q_{II}^{D} was formed far from the open edge.[19,20] (c) The polycrystal region in (b) was cut off; the remaining part consisted of only the single crystal region. (d) The single crystal region was soaked in 20% PEG-4K. PEG-4K diffused slowly into the capillary from the open edge, and a single crystal region of Q_{II}^{G} was gradually formed. X-ray diffraction patterns were obtained from the Q_{II}^{D}−Q_{II}^{G} interface (red arrow) and 0.5 mm above and below the interface.

Figure 3 shows X-ray diffraction images of the Q_{II}^{D}−Q_{II}^{G} interface in the capillary sample (Supporting Information Figure S1). Analysis of the X-ray diffraction spots indicated that at 4.5 mm from the edge of the capillary facing the PEG-4K solution (Figures 3a and 3d) the single crystal of the Q_{II}^{D} phase only existed in the exposed region, and the orientation of the single crystal could be determined. At 4.0 mm from the edge (Figures 3b and 3e), spots from the Q_{II}^{D} phase were still observed, and some new spots appeared. At 3.5 mm from the edge (Figures 3c and 3f), spots from the Q_{II}^{D} phase disappeared, and only the new spots at 4.0 mm were observed. The ratio of the distance of spots from the beam center

DOI: 10.1021/acs.langmuir.5b02180
Langmuir 2015, 31, 11353−11359

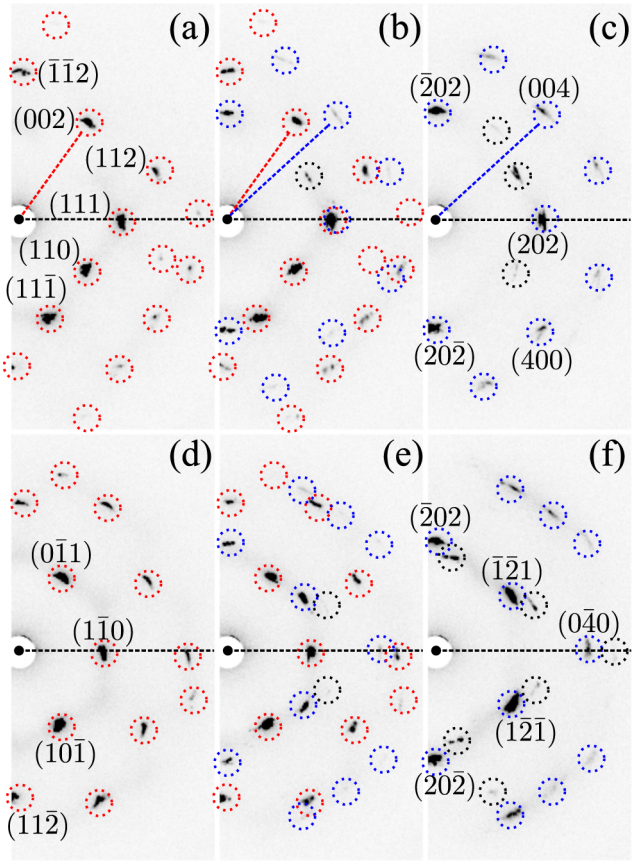

Figure 3. X-ray diffraction images of the capillary sample at around the Q_{II}^{D}–Q_{II}^{G} interface in 20% PEG-4K. The images represent cumulative data of rotational angles (a–c) from 30° to 40° and (d–f) from 120° to 130°. Only the right halves of the images are shown because the original images are centrosymmetric. (a, d) At 4.5 mm from the edge facing 20% PEG-4K. (b, e) At 4.0 mm. (c, f) At 3.5 mm. Diffraction spots of the Q_{II}^{D} phase are seen in (a) and (d), and those of Q_{II}^{G} are in (c) and (f). Diffraction spots from the both phases can be seen in (b) and (e). Diffraction spots from the Q_{II}^{D} and Q_{II}^{G} phases have been indicated by dashed red and blue circles, respectively. Some Miller indices of the Q_{II}^{D} phase are assigned in (a) and (d), and those of Q_{II}^{G} are assigned in (c) and (f). A beam center is located at the left end of the horizontal line in each image. Dashed lines are drawn from the beam center to spots of the (002) plane of Q_{II}^{D} and to spots of the (004) plane of Q_{II}^{G} in (a–c): the dashed lines of Q_{II}^{D} are red, while those of Q_{II}^{G} are blue. Dashed back circles were diffraction spots from small crystal(s) in the Q_{II}^{G} phase. The intensities of the spots from the small crystal(s) are less than one-tenth of that of the large single crystal of the Q_{II}^{G} which could be assigned Miller indexes.

indicates that the phase observed at 3.5 mm was Q_{II}^{G}. Using the diffraction spot positions at 3.5 mm, one orientation of single crystals of the Q_{II}^{G} phases was determined. Moreover, orientations of both phases at 4.0 mm could be determined. The orientations of the Q_{II}^{D} and Q_{II}^{G} phases at 4.0 mm were almost the same as those of Q_{II}^{D} at 4.5 mm and Q_{II}^{G} at 3.5 mm, respectively. Some of the Miller indices are shown in Figure 3. Some weak spots were observed at positions where no spots appeared from the single crystal of the Q_{II}^{G} phase (Figures 3c and 3f). But the distance relation between the weak spots and a beam center satisfied that of the Q_{II}^{G} phase. Thus, I concluded that there was one large single crystal and smaller crystal(s) of the Q_{II}^{G} phase with different orientations. But the intensities of those peaks from the small crystal(s) were less than one-tenth of that of the large single crystal. Red dashed lines are drawn from the beam center to spots of the (002) plane of Q_{II}^{D} in Figure 3a,b, and blue are drawn to spots of the (004) plane of Q_{II}^{G} in Figure 3b,c. However, the directions are slightly different. This means that the [002] direction of the crystallographic orientation of Q_{II}^{D} is close, but not identical, to the [004] direction of Q_{II}^{G}. The angle between the two directions is about 10° (Figure 3b). A diffraction spot from the (111) plane of Q_{II}^{D} and a spot from the (202) plane of Q_{II}^{G} were observed on the horizontal line from the beam center in Figure 3b. Spots of the (1$\bar{1}$0) plane of Q_{II}^{D} and the (0$\bar{4}$0) plane of Q_{II}^{G} lie on the horizontal line in Figure 3e. These results indicate that the corresponding directions of the single crystals in both phases are almost the same and parallel to the horizontal plane. The lattice constants of the Q_{II}^{D} and Q_{II}^{G} phases are 8.9 and 14.0 nm, respectively. The ratio of these lattice constants is 1.57, which agrees well with the theoretical value of 1.58.[25,26] Thus, a ratio of volumes between the Q_{II}^{D} and Q_{II}^{G} phases was almost the same or decreased slightly (~2%) in the phase transition.[25]

The diffraction spots appearing in X-ray images (Figure 3 or Figure S1) could be considered as reciprocal lattice points on an Ewald sphere.[27] The positions of the diffraction spots in the two-dimensional images were converted to the positions of the reciprocal lattice points (Figure 4). Figure 4a is the view from the [040] direction of the Q_{II}^{G} phase, which almost corresponds to the [$\bar{1}$10] direction of the Q_{II}^{D} phase. Figure 4b is the view from the [002] direction of Q_{II}^{D}, which is close

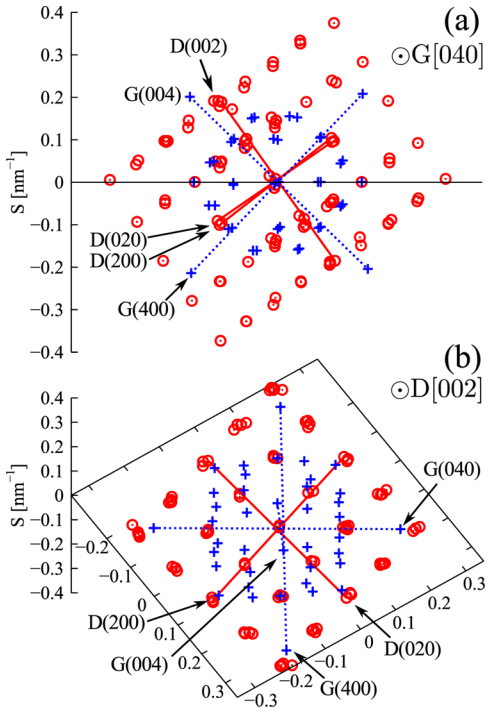

Figure 4. Reciprocal lattice of the Q_{II}^{D} (red circles) and Q_{II}^{G} (blue crosses) phases calculated from peak positions of X-ray diffraction spots. The points that satisfy $|h|, |k|, |l| \leq 2$ (h, k, and l are the Miller indices) and the {400} planes of the Q_{II}^{G} phase are shown. Solid red and dotted blue lines are drawn to connect lattice points from respectively the {200} planes of Q_{II}^{D} and the {400} planes of Q_{II}^{G} to the origin. (a) View from [040] direction of Q_{II}^{G}. (b) From [002] direction of Q_{II}^{D}. Some lattice points from the {200} planes of Q_{II}^{D} and the {400} planes of Q_{II}^{G} have been indexed.

DOI: 10.1021/acs.langmuir.5b02180
Langmuir 2015, 31, 11353–11359

to the [004] direction of Q_{II}^{G}. Figure 4b shows that the angle between the lines of Q_{II}^{D} (200) and Q_{II}^{G} (400) is about 45°, as is the angle between Q_{II}^{D} (020) and Q_{II}^{G} (040). These results indicate that the crystallographic orientation of the Q_{II}^{G} phase rotates by almost 45° with respect to that of the Q_{II}^{D} phase around the [002] axis of Q_{II}^{D} or the [004] axis of Q_{II}^{G}. The [004] direction of Q_{II}^{G}, however, tilts by about 10° from the [002] direction of Q_{II}^{D} (Figure 4a). The rotation matrix from Q_{II}^{D} to Q_{II}^{G}, R_{DG}, was calculated from the positions of the X-ray diffraction spots. The normalized rotational axis of R_{DP} was [−0.101 0.198 0.975], and the calculated rotational angle of the matrix was 47°. A theoretical rotational matrix that converted the [111] direction into [202] and [1$\bar{1}$0] into [0$\bar{4}$0] was calculated as well. The relationships that defined this matrix were found in the Q_{II}^{D}−Q_{II}^{G} phase transition (Figures 3 and 4). The rotational axis of this theoretical matrix was [−0.083 0.201 0.976], and its rotational angle was 46°. These values were fairly close to those calculated from the diffraction spots positions. Therefore, I concluded that during the phase transition from Q_{II}^{D} to Q_{II}^{G} the crystallographic orientation rotated by 46° around the [−0.083 0.201 0.976] axis. The [111] and [1$\bar{1}$0] directions of the Q_{II}^{D} phase corresponded to the [202] and [0$\bar{4}$0] directions of the Q_{II}^{G} phase, respectively.

Figures 5a and 5b show the orientation relationship between the Q_{II}^{D} and Q_{II}^{G} phases, as observed in the present experiments. Figure 5a is a view from the [$\bar{1}$10] direction of the Q_{II}^{D} phase, while Figure 5b is a view from the [010] direction of the Q_{II}^{G} phase. These two directions lie along the horizontal line at the Q_{II}^{D}−Q_{II}^{G} transition interface (Figure 3e). Other directions that lie along the horizontal line are the [111] of Q_{II}^{D} and the [202] of Q_{II}^{G} (Figure 3b), which are parallel to the direction of the water channel in the respective phases (Figures 5a and 5b). Thus, I concluded that the water channels in the [111] direction of the Q_{II}^{D} phase and the [101] direction of the Q_{II}^{G} phase are preserved during the Q_{II}^{D}−Q_{II}^{G} phase transition. Using this orientation relationship, I propose a model of this phase transition. The model has two important features: (1) All four-way junctions (e.g., A) in the Q_{II}^{D} phase separate into 2 three-way junctions (e.g., A−A′) in Q_{II}^{G}, and the freshly formed water channels between the two three-way junctions are perpendicular to the [001] direction in the Q_{II}^{D} or Q_{II}^{G} phase. (2) The [111] direction of water channels in the Q_{II}^{D} phase is preserved in the Q_{II}^{G} phase, but the Miller index of the direction becomes [101] (which is parallel to [202]) in the Q_{II}^{G} phase because the crystallographic orientation changes during the transition. The phase transition starts from the Q_{II}^{D} phase in Figure 5a, and the intermediate structure is shown in Figure 5c. Then, the structure finally transforms into the Q_{II}^{G} phase in Figure 5d, which has the same orientation as in Figure 5b. Thus, the [001] direction of the Q_{II}^{G} phase tilts by 10° toward the [101] direction of the Q_{II}^{G} phase or the [111] direction of the Q_{II}^{D} phase according to feature (2) above. I only treat the transformation of water channels explicitly, but the lipid surface also changes with the water channels.

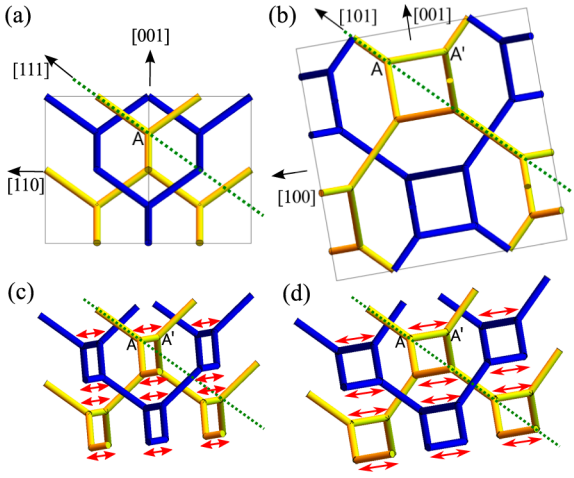

Figure 5. Orientation relationship in transition from (a) the Q_{II}^{D} phase to (b) the Q_{II}^{G} phase. Pipes indicate the centers of the water channels. The different tones of pipes indicate the two distinct water channels. Models are viewed from the [$\bar{1}$10] direction of Q_{II}^{D} in (a) and the [010] direction of Q_{II}^{G} in (b). Unit cells of 2 × 2 × 2 (a) and a single unit cell (b) are drawn. All four-way junctions (e.g., A in (a)) of the Q_{II}^{D} phase are transformed into pairs of three-way junctions (e.g., A−A′ in (b)) of the Q_{II}^{G} phase. Newly appearing pipes are perpendicular to the [001] direction of the Q_{II}^{G} phase (b). The [111] direction of water channels in the Q_{II}^{D} phase is fixed during the phase transition (dotted green line) but becomes [101] in the Q_{II}^{G} phase because the crystallographic orientation changes during the Q_{II}^{D}−Q_{II}^{G} transition. Thus, in the Q_{II}^{D}−Q_{II}^{G} phase transition, the crystallographic orientation rotates by 45° around the [001] direction and by about 10° around the [01$\bar{1}$] direction of Q_{II}^{D}. The hypothetical intermediate of the transformation shown in (c) has transformed into Q_{II}^{G} in (d).

DISCUSSION

To make a single crystal region of Q_{II}^{D} phase with monoolein, I used a method which I reported previously.[19,20] In the method, L_3 phase with 20% tBA in a capillary was soaked into water. The tBA diffused out from the open edge of the capillary, and the L_3 phase transformed into the Q_{II}^{D} phase. After one or two weeks, a single crystal region was formed at far from the open edge. The mechanism of the single crystallization would be almost the same as macromolecular crystallization with the counter-diffusion method.[28] The Q_{II} phases have water channels typically 2−5 nm in diameter.[16] The diffusion process in the water channels is therefore fairly slower than bulk solution. Moreover, direction of the diffusion is limited to the capillary axis direction. Slow diffusion out of an additive from the open edge of the Q_{II}^{D} capillary sample makes a gradient of additive concentration which is important for single crystallization.[19,28] I left the capillary in water about two months to reduce the effect of tBA in the Q_{II}^{D}−Q_{II}^{G} phase transition. A lattice constant of the Q_{II}^{D} phase from the single crystal region was about 9.8 nm. Cherezov et al. have studied effect of tBA on phases of monoolein and shown a proportional relation between lattice constants of Q_{II}^{D} phases and tBA concentrations.[29] A lattice constant of the Q_{II}^{D} phase without tBA in their data was about 10 nm, which was almost the same as that in the single crystal region. Thus, tBA concentration at the single crystal region after two months soaking was almost 0%.

High-molecular-weight PEG solutions are known to convert the Q_{II}^{D} phase of monoolein into the Q_{II}^{G} phase.[22−24] This reflects the water-withdrawing effect of high-molecular-weight PEG, which are considered to be excluded from the aqueous matrix of the cubic phase.[24,30] PEG-4K solution made a gradient of lattice constant in the capillary sample and caused the Q_{II}^{D}−Q_{II}^{G} phase transition (Figure S2). In the previous paper,[20] I observed very slow Q_{II}^{D}−Q_{II}^{P} phase transition in a single crystal region of a capillary sample using 10 mM L-arginine solution. It took about 8 h for the capillary sample at 3.5 mm from the edge to change its phase from Q_{II}^{D} to Q_{II}^{P}.

DOI: 10.1021/acs.langmuir.5b02180
Langmuir 2015, 31, 11353−11359

This result indicated advance speed of phase transition along the capillary at 3.5 mm was about 0.06 mm/hour (~0.5 mm (beam diameter)/8 h). In this paper, I applied almost the same method to observe Q_{II}^{D}−Q_{II}^{G} phase transition. I soaked the open edge of the capillary sample contained a single crystal region of the Q_{II}^{D} phase into PEG-4K solution. After 1 day, I found the phase of the sample located at the open edge was transformed into the Q_{II}^{G}, and the interface between Q_{II}^{D} and Q_{II}^{G} was 4.0 mm from the open edge. After 3 days, the interface moved to 7.0 mm from the open edge. Therefore, the advance speed of the phase transition in the capillary sample was 1−4 mm/day, and the speed became slower as the distance from the open edge became larger. The advance speeds in capillary samples of other experiments were the same or less. These results indicated phase transition process were slow enough to be observed with the technique I used in this paper.

I took a sample capillary from PEG-4K solution and measured X-ray diffraction. The total measurement time was about 3 h. But I did not observe any time-dependent change or deterioration in X-ray diffraction of the sample during the measurement. The sample was stable enough to measure X-ray diffraction images. I think the stability comes from slow diffusion of solution in the Q_{II} phases of the capillary samples. Additive concentration around or in the monoolein affects the phase. But the measurement time was short for the additive to change its concentration in the capillary sample. Therefore, taking out from PEG-4K solution did not affect the Q_{II}^{D}−Q_{II}^{G} interface in the capillary sample. Moreover, crystallographic orientations of the Q_{II}^{G} at 4.0 and 3.5 mm were the same. This result indicated the capillary sample kept crystallographic orientation even if the phase transition advanced along the capillary axis direction.

The transformation of TPMS structures from D to G has been studied theoretically.[12−15] Fogden, Shröder, and Hyde have proposed a tetragonal pathway model for the D−G transformation that preserves the topology and zero mean curvature throughout.[14,15] On the basis of the tetragonal pathway model, Squires et al. developed a pictorial model of the Q_{II}^{D}−Q_{II}^{G} transition in which the rotational axis of crystal orientation was the [00l] axis and the rotational angle was calculated to be 45°.[31] According to the Squires' model, the [002] direction of the Q_{II}^{D} phase and the [004] direction of the Q_{II}^{G} phase must be parallel. This relationship, which agrees with the first of the two features of my model described above, was confirmed by X-ray diffraction of the oriented Q_{II} phase of the monoolein sample;[18] however, the angle resolution of that particular setup was not enough to describe the details of the orientation relationship in the Q_{II}^{D}−Q_{II}^{G} transition. My data clearly indicate that the [004] direction of the Q_{II}^{G} phase tilts by 10° from the [002] direction of the Q_{II}^{D} phase (Figures 3b and 4). This small but significant tilt indicates that the [111] direction of the Q_{II}^{D} phase corresponds to the [101] direction of the Q_{II}^{G} phase in the phase transition. This is how the second feature of my model arose. Thin films studies have revealed the same orientation relationship between the {111} planes in the Q_{II}^{D} phase and the {220} planes in the Q_{II}^{G} phase during the phase transition.[17,32] A rhombohedral pathway model has also been proposed for the D−G transformation.[14,15] In this pathway, the P surface appears as an intermediate. Transformation via the rhombohedral pathway was expected to preserve the relative axes of the respective Q_{II}^{D} and Q_{II}^{G} cubic unit cells,[18] but this relationship did not agree with my experiment. The tetragonal pathway, considered to be theoretically more favorable than the rhombohedral pathway in terms of curvature and packing homogeneity, was more suitable for the D−G transformation.[15]

I repeated the same experiments with another single crystal regions of the Q_{II}^{D} phase. Each of the single crystal samples had a different orientation to the capillary because I could not control the crystallographic orientation of the single crystal in the capillary.[19] Thus, I could use different orientations of the samples to the direction of the phase transition advanced which was parallel to the capillary axis. In these samples, I also found the same orientational relation in the Q_{II}^{D}−Q_{II}^{G} transition (Figures 5a and 5b). In some cases, two orientations of single crystals of the Q_{II}^{G} phase were found, but the two orientations still satisfied the same orientational relation. I therefore concluded the crystallographic orientation of the single crystal region in the capillary did not affect orientational relation in the Q_{II}^{D}−Q_{II}^{G} phase transition.

In the Q_{II}^{D}−Q_{II}^{G} phase transition, I showed [111] axis of the Q_{II}^{D} was converted to [101] axis of the Q_{II}^{G} (Figures 5a and 5b). The symmetry of the Q_{II}^{D} is cubic. It means eight axes in ⟨111⟩ axes set are equivalent. Thus, eight orientations of the Q_{II}^{G} could be produced from a single (orientation) crystal of the Q_{II}^{D} phase. But I observed one major orientation of the Q_{II}^{G} (Figure 3). Therefore, the crystallographic orientation of the Q_{II}^{D} phase in the present paper would restrict transformation to other orientations of the Q_{II}^{G} phase. In these experiments, a PEG-4K solution was used to induce phase transition of the sample in capillary. Thus, the phase transition advanced in one direction along the capillary axis from the open end of the capillary located at the bottom. The [111] and [1$\bar{1}$0] directions of the Q_{II}^{D} phase were perpendicular to this capillary axis. The [111] direction of the Q_{II}^{D} phase was the direction of the water channel preserved during the phase transition. Thus, the angular relationship between the direction of the preserved water channel and the direction of advancing phase transition would affect the orientation choice of the Q_{II}^{G} phase in the D−G transition. The same tendency was observed in the Q_{II}^{D}−Q_{II}^{P} transition study using the single crystal region.[20]

In the tetragonal pathway model of the D−G transition, the *c*-axis length of the tetragonal unit cell decreases by 20% and the *a*-axis length increases by 13%.[33] This indicates that the length of the [001] direction of D shrinks by 20% in G, while the length of the direction perpendicular to the [001] expands by 13%. In the rhombohedral pathway model of the D−G transition, however, the *c*-axis length of the rhombohedral unit cell decreases by 61% and the *a*-axis length increases by 61%.[33] This indicates that the length of the [111] direction of D shrinks by 61% in G, while the length of the direction perpendicular to the [111] expands. The single crystal of the Q_{II}^{D} phase is a liquid crystal, and thus, the membrane surface and water channels are mobile during the phase transition. But a large length change in one direction would damage the single crystal. The length change in the rhombohedral pathway is particularly large, which would hinder transformation via the rhombohedral pathway in the D−G transition of the monoolein−water system. The changes in axis lengths would inevitably deteriorate the single crystal region and/or cause discontinuities in the membrane surface.

My previous paper presented an orientation relationship in which one direction of the water channel was preserved during the Q_{II}^{D}−Q_{II}^{P} transition,[20] and the same relationship was observed again in the Q_{II}^{D}−Q_{II}^{G} transition. However, there is no direct information about the phase transition intermediate

DOI: 10.1021/acs.langmuir.5b02180
Langmuir 2015, 31, 11353−11359

between the Q_{II} phases. Thus, further experimental studies are essential to understand the phase transitions between the Q_{II} phases. The hypothetical intermediate in Figure 5c has tetragonal symmetry. Thus, my transition model seems to agree well with the tetragonal pathway model.[14,15] Because the tetragonal pathway model was developed on the basis of a few unit cells, the model seems to tolerate the rotation of the unit cell. It is, however, difficult to apply the tetragonal pathway model directly to connecting the Q_{II}^{D} and Q_{II}^{G} phases because the rotation and shrinkage or expansion of unit cell(s) were not taken into account. Thus, further theoretical and experimental work needs to be conducted on the interfaces of the Q_{II} phases.

CONCLUSION

By using the single crystal region of the Q_{II} phase of monoolein, I determined the orientation relationships in the Q_{II}^{D}−Q_{II}^{G} phase transition. The [111] and [1$\bar{1}$0] directions of the Q_{II}^{D} phase corresponded to the [202] and [0$\bar{4}$0] directions of the Q_{II}^{G} phase, respectively. Using these relationships, I proposed a new transformation model that was similar to a previously published model[18,31] based on a theoretical tetragonal pathway.[9,10] The present model differs from the previous model in that one of the water channel directions is preserved while another appears. The preservation of one direction of the water channels has also been observed in the Q_{II}^{D}−Q_{II}^{P} phase transition.[20] The present results represent the second demonstration of the benefits of the single-crystallization technique of the Q_{II} phase.[19]

ASSOCIATED CONTENT

Supporting Information

The Supporting Information is available free of charge on the ACS Publications website at DOI: 10.1021/acs.langmuir.5b02180.

Sequential X-ray diffraction images for Figure 3; lattice constants of the Q_{II}^{D} and Q_{II}^{G} phases in a capillary sample (PDF)

AUTHOR INFORMATION

Corresponding Author

*E-mail oka.toshihiko@shizuoka.ac.jp.

Notes

The authors declare no competing financial interest.

ACKNOWLEDGMENTS

This work was supported by JSPS KAKENHI Grant 15K05243. I am grateful to Prof. Hyde and Prof. Yamazaki for helpful discussions.

REFERENCES

(1) Hyde, S.; Ninham, B.; Andersson, S.; Larsson, K.; Landh, T.; Blum, Z.; Lidin, S. The Mathematics of Curvature. *The Language of Shape*; Elsevier: Amsterdam, 1997; pp 1−42.

(2) Lord, E. A.; Mackay, A. L. Periodic Minimal Surfaces of Cubic Symmetry. *Curr. Sci.* **2003**, *85* (3), 346−362.

(3) Seddon, J. M.; Templer, R. H. *Structure and Dynamics of Membranes*; North-Holland: Amsterdam, 1995; Vol. *1*, pp 97−160.

(4) Yamazaki, M. *Advances Planar Lipid Bilayers and Liposomes*; Academic Press: New York, 2009; Vol. *9*, pp 163−209.

(5) Hajduk, D. A.; Harper, P. E.; Gruner, S. M.; Honeker, C. C.; Kim, G.; Thomas, E. L.; Fetters, L. J. The Gyroid: A New Equilibrium Morphology in Weakly Segregated Diblock Copolymers. *Macromolecules* **1994**, *27* (15), 4063−4075.

(6) Murakami, S.; Yamada, N.; Nagano, M.; Osumi, M. Three-Dimensional Structure of the Prolamellar Body in Squash Etioplasts. *Protoplasma* **1985**, *128* (2−3), 147−156.

(7) Almsherqi, Z. A.; Kohlwein, S. D.; Deng, Y. Cubic Membranes: A Legend beyond the Flatland* of Cell Membrane Organization. *J. Cell Biol.* **2006**, *173* (6), 839−844.

(8) Michielsen, K.; Stavenga, D. G. Gyroid Cuticular Structures in Butterfly Wing Scales: Biological Photonic Crystals. *J. R. Soc., Interface* **2008**, *5* (18), 85−94.

(9) Chu, C.-Y.; Lin, W.-F.; Tsai, J.-C.; Lai, C.-S.; Lo, S.-C.; Chen, H.-L.; Hashimoto, T. Order−Order Transition between Equilibrium Ordered Bicontinuous Nanostructures of Double Diamond and Double Gyroid in Stereoregular Block Copolymer. *Macromolecules* **2012**, *45* (5), 2471−2477.

(10) Takagi, H.; Yamamoto, K.; Okamoto, S. Ordered-Bicontinuous-Double-Diamond Structure in Block Copolymer/homopolymer Blends. *EPL Europhys. Lett.* **2015**, *110* (4), 48003.

(11) Chu, C. Y.; Jiang, X.; Jinnai, H.; Pei, R. Y.; Lin, W. F.; Tsai, J. C.; Chen, H. L. Real-Space Evidence of the Equilibrium Ordered Bicontinuous Double Diamond Structure of a Diblock Copolymer. *Soft Matter* **2015**, *11* (10), 1871−1876.

(12) Sadoc, J. F.; Charvolin, J. Infinite Periodic Minimal Surfaces and Their Crystallography in the Hyperbolic Plane. *Acta Crystallogr., Sect. A: Found. Crystallogr.* **1989**, *45* (1), 10−20.

(13) Benedicto, A. D.; O'Brien, D. F. Bicontinuous Cubic Morphologies in Block Copolymers and Amphiphile/Water Systems: Mathematical Description through the Minimal Surfaces. *Macromolecules* **1997**, *30* (11), 3395−3402.

(14) Fogden, A.; Hyde, S. T. Continuous Transformations of Cubic Minimal Surfaces. *Eur. Phys. J. B* **1999**, *7*, 91−104.

(15) Schröder-Turk, G. E.; Fogden, A.; Hyde, S. T. Bicontinuous Geometries and Molecular Self-Assembly: Comparison of Local Curvature and Global Packing Variations in Genus-Three Cubic, Tetragonal and Rhombohedral Surfaces. *Eur. Phys. J. B* **2006**, *54*, 509−524.

(16) Seddon, A. M.; Lotze, G.; Plivelic, T. S.; Squires, A. M. A Highly Oriented Cubic Phase Formed by Lipids under Shear. *J. Am. Chem. Soc.* **2011**, *133* (35), 13860−13863.

(17) Rittman, M.; Amenitsch, H.; Rappolt, M.; Sartori, B.; O'Driscoll, B. M. D.; Squires, A. M. Control and Analysis of Oriented Thin Films of Lipid Inverse Bicontinuous Cubic Phases Using Grazing Incidence Small-Angle X-Ray Scattering. *Langmuir* **2013**, *29* (31), 9874−9880.

(18) Seddon, A. M.; Hallett, J.; Beddoes, C.; Plivelic, T. S.; Squires, A. M. Experimental Confirmation of Transformation Pathways between Inverse Double Diamond and Gyroid Cubic Phases. *Langmuir* **2014**, *30* (20), 5705−5710.

(19) Oka, T.; Hojo, H. Single Crystallization of an Inverse Bicontinuous Cubic Phase of a Lipid. *Langmuir* **2014**, *30* (28), 8253−8257.

(20) Oka, T. Transformation between Inverse Bicontinuous Cubic Phases of a Lipid from Diamond to Primitive. *Langmuir* **2015**, *31* (10), 3180−3185.

(21) Goldstein, H. *Classical Mechanics*; Addison-Wesley Pub. Co.: Reading, MA, 1980.

(22) Masum, S. M.; Li, S. J.; Awad, T. S.; Yamazaki, M. Effect of Positively Charged Short Peptides on Stability of Cubic Phases of Monoolein/Dioleoylphosphatidic Acid Mixtures. *Langmuir* **2005**, *21* (12), 5290−5297.

(23) Chung, H.; Caffrey, M. The Curvature Elastic-Energy Function of the Lipid−water Cubic Mesophase. *Nature* **1994**, *368* (6468), 224−226.

(24) Conn, C. E.; Darmanin, C.; Mulet, X.; Hawley, A.; Drummond, C. J. Effect of Lipid Architecture on Cubic Phase Susceptibility to Crystallisation Screens. *Soft Matter* **2012**, *8* (26), 6884−6896.

(25) Hyde, S. T.; Andersson, S.; Bodil, E.; Kåre, L. A Cubic Structure Consisting of a Lipid Bilayer Forming an Infinite Periodic Minimum Surface of the Gyroid Type in the Glycerolmonooleat-Water System. *Z. Kristallogr.* **1984**, *168*, 213−219.

DOI: 10.1021/acs.langmuir.5b02180
Langmuir 2015, 31, 11353−11359

(26) Templer, R. H.; Seddon, J. M.; Warrender, N. A. Measuring the Elastic Parameters for Inverse Bicontinuous Cubic Phases. *Biophys. Chem.* **1994**, *49* (1), 1−12.
(27) Warren, B. E. *X-Ray Diffraction*; Courier Corporation: North Chelmsford, MA, 1969.
(28) García-Ruiz, J. M. Counterdiffusion Methods for Macromolecular Crystallization. In *Methods in Enzymology*; Charles, W., Carter, J. R. M. S., Eds.; Macromolecular Crystallography, Part C; Academic Press: New York, 2003; Vol. *368*, pp 130−154.
(29) Cherezov, V.; Clogston, J.; Papiz, M. Z.; Caffrey, M. Room to Move: Crystallizing Membrane Proteins in Swollen Lipidic Mesophases. *J. Mol. Biol.* **2006**, *357* (5), 1605−1618.
(30) Cherezov, V.; Fersi, H.; Caffrey, M. Crystallization Screens: Compatibility with the Lipidic Cubic Phase for in Meso Crystallization of Membrane Proteins. *Biophys. J.* **2001**, *81* (1), 225−242.
(31) Squires, A. M.; Templer, R. H.; Seddon, J. M.; Woenkhaus, J.; Winter, R.; Narayanan, T.; Finet, S. Kinetics and Mechanism of the Interconversion of Inverse Bicontinuous Cubic Mesophases. *Phys. Rev. E* **2005**, *72* (1), 011502.
(32) Rappolt, M.; Gregorio, G. M. D.; Almgren, M.; Amenitsch, H.; Pabst, G.; Laggner, P.; Mariani, P. Non-Equilibrium Formation of the Cubic Pn 3 M Phase in a Monoolein/water System. *Europhys. Lett. EPL* **2006**, *75* (2), 267−273.
(33) Hyde, S. T. Personal communication, 2015.

DOI: 10.1021/acs.langmuir.5b02180
Langmuir 2015, 31, 11353−11359